J. Fluid Mech. (1996), *vol.* 315, *pp.* 345–365

Dynamic simulation of hydrodynamically interacting spheres in a quiescent second-order fluid

By RONALD J. PHILLIPS

Department of Chemical Engineering and Materials Science, University of California, Davis, Davis, CA 95616, USA

(Received 11 August 1994 and in revised form 29 December 1995)

A method is described for calculating the motion of N spherical particles suspended in a quiescent second-order fluid. The method requires calculation of only the low-Reynolds-number Newtonian velocity profile. This profile is used in conjunction with what has been called the 'Reciprocal theorem method' to evaluate particle velocities accurate to leading order in the Deborah number. If the Newtonian velocity field is found by a multipole moment expansion, then it is shown that the method can be integrated neatly into the Stokesian dynamics method of simulating Newtonian suspensions. Simulation results involving two, three, four and six particles are reported as illustrative examples, and are compared with corresponding results for particles in Newtonian fluids and with experimental results found in the literature. In addition, simulations of sedimenting suspensions are performed by using periodic boundary conditions to model an unbounded system, and the observed formation of clusters in the sedimenting system is shown to be in qualitative agreement with experimental observations.

1. Introduction

The motion of small particles in viscous fluids is of fundamental interest in areas such as microhydrodynamics (Kim & Karrila 1991) and colloid science (Russel, Saville & Schowalter 1989), and is of practical interest in a number of suspension-processing operations. Methods for calculating hydrodynamic interactions between N suspended particles have been a subject of intensive research for some time, and several approaches have been developed, including the method of reflections (Happel & Brenner 1986), boundary collocation (Ganatos, Pfeffer & Weinbaum 1978), boundary integral formulations (Kim & Karrila 1991) and Stokesian Dynamics (Brady & Bossis 1988), the latter being closely related to the method of multipole moments (Weinbaum, Ganatos & Zong-Yi 1990). However, because of the complexity of N-body low-Reynolds-number hydrodynamics problems, relatively little work has been done to incorporate effects due to inertia or non-Newtonian behaviour into these methods of solution. In this work the effect on particle motion of weak elasticity in the suspending fluid is examined and comparisons are made with the corresponding low-Reynolds-number Newtonian case and with experimental observations.

In contrast to the N-body problem, a significant amount of theoretical work has been done to understand the effect of elasticity on the motion of a single spherical or non-spherical particle in various flow fields. Reviews that discuss much of that work, particularly the results obtained by perturbation methods, have been given by Leal (1979) and Brunn (1980). Many of these investigations make use of the second-order fluid constitutive equation, which becomes valid in the limit where the Deborah

number *De*, defined as the ratio of the fluid relaxation time to the time scale of a given flow, approaches zero. The second-order fluid constitutive equation is one of a series of constitutive equations obtained by the retarded motion expansion (Bird, Armstrong & Hassaguer 1987). Although few if any fluids can be classed as 'second-order fluids', most well-known constitutive models reduce to the retarded motion expansion in the limit of low Deborah number. It is therefore expected that useful qualitative information can be obtained through use of the second-order result. In addition, it is useful to examine theoretically the effects of weak elasticity in the absence of shear-thinning, even if such systems are difficult to realize in practice. Numerical results that were obtained for flow around a single sphere that are valid at higher Deborah numbers and which account for shear-thinning in the suspending fluid are also available (i.e. Lunsmann *et al.* 1993; Bush & Phan-Thien 1984; Chhabra & Uhlherr, 1980).

It is interesting to compare results predicted for particle motion in second-order (low-*De*) and Newtonian (zero-*De*) fluids under conditions of zero Reynolds number, many results for the latter case being required by the reversibility condition for Stokes flow. In a Newtonian fluid, a spherical particle suspended in a unidirectional shear flow does not migrate across streamlines, and a sedimenting, transversely isotropic particle maintains its initial orientation. In contrast, in a second-order fluid the spherical particle migrates in the direction of decreasing shear rate (Chan & Leal 1977) and the sedimenting particle orients itself such that its axis of revolution is in the direction of sedimentation (Kim 1986). Finally, in a second-order fluid the well-known Jeffrey orbits of ellipsoidal particles in shear flows are altered such that the particles drift towards a preferred orbit (Leal 1975).

A number of these theoretical results have provided an explanation for behaviour observed experimentally. Lateral migration across streamlines has been observed in Couette and Poiseuille flows, and the fact that non-spherical particles assume a preferred orbit when rotating in a shear flow in viscoelastic fluids was shown in a series of studies by Mason and co-workers (Gauthier, Goldsmith & Mason 1971; Karnis & Mason, 1967; Bartram, Goldsmith & Mason 1975). Also, the tendency of particles to settle in the direction of their axis of rotation in fluids exhibiting elasticity, providing inertial effects are negligible, is well-established (Chiba, Song & Horikawa 1986; Liu & Joseph 1993).

The area of two- or multi-particle dynamics in viscoelastic fluids is not as well-studied as the single particle case, but some useful and interesting results are available, of which we mention but a few. Michele, Patzold & Donis (1977) showed that, when subjected to an oscillating shear flow, spherical particles align in rows that grow progressively longer over time. This observation is consistent with the earlier work by Highgate & Whorlow (1969), and it has since been shown that the direction of alignment can be affected by the relative importance of elastic and inertial effects (Petit & Noetinger 1988). Riddle, Narvaez & Bird (1977) showed that two spheres sedimenting in a tube move together or apart depending on whether their initial separation is less or greater than a critical value. With regard to theoretical work, the only multiparticle results available for second-order fluids are asymptotic results calculated by Brunn (1977*a*, *b*, 1980). Brunn shows that particles sedimenting in a quiescent, unbounded second-order fluid move together to form a doublet, which is oriented such that sedimentation occurs in the direction of the line joining the two sphere centres.

Some experimental observations for spheres sedimenting in otherwise quiescent viscoelastic fluids are particularly relevant to this work. Joseph *et al.* (1992, 1994) show

photographs in which sedimenting spheres form elongated aggregates and, in many cases, chains that are many spheres long. The elongation is in the direction of sedimentation for viscous-dominated systems and is perpendicular to the direction of sedimentation when inertia becomes important. Allen & Uhlherr (1989) studied sedimentation in viscoelastic fluids by backlighting the cell containing the suspension and taking photographs. In a Newtonian fluid, a monomodal suspension settles homogeneously with a sharp interface between the suspension and supernatant. In contrast, when the fluid is viscoelastic, very often both globular and 'finger-like' particle-rich and particle-depleted regions are observed, and no sharp interface is formed.

In this paper, a method is described for calculating the interactions between N spherical particles in a second-order fluid. The approach makes use of what Brunn (1980) has termed the 'Reciprocal theorem method', which requires knowledge of only the Newtonian velocity field. A similar approach has been used to study the effects of a small amount of inertia on the force on a rigid particle (Lovalenti & Brady 1993). It is valid in principle for arbitrary sphere locations, being limited in practical terms only by the accuracy of the Newtonian velocity field that is used. Here that velocity field is obtained by a multipole moment expansion. The correction terms needed to account for elasticity are then readily incorporated into Stokesian dynamics simulations, allowing comparisons to be made with earlier Newtonian results and raising the possibility of dynamically simulating suspensions at low Deborah number under various flow conditions.

The organization of the paper is as follows. In §2 the governing equations are presented and separated into zero- and first-order components by perturbation analysis. The methods for solution for the Newtonian case and for the equations governing the non-Newtonian terms are outlined in §3. The methods are applied to two- and multi-sphere problems in §4, and comparisons are made with earlier results and experimental observations found in the literature. In particular, direct comparisons are made with three- and four-sphere simulation results reported by Durlofsky, Brady & Bossis (1987), and qualitative comparisons are made with the observations of Joseph *et al.* (1992, 1994) and Allen & Uhlherr (1989).

2. Problem formulation

We consider N identical spheres with radius a and surfaces denoted by $S_1, S_2, \ldots, S_N$. The spheres are all subject to the same gravitational force, are free of any applied torque, and are suspended in a viscoelastic fluid. The objective is to compute the sphere velocities to $O(De)$ for arbitrary sphere positions, assuming a second-order constitutive model for the fluid. Here we define the Deborah number for the sedimentation process by

$$De_s = \frac{\lambda}{\tau_s} = \lambda\left(\frac{2a(\rho_p - \rho_f)}{9\eta_0}\right). \tag{1}$$

In (1), the parameter λ is the relaxation time for the fluid, τ_s is the time for a single, isolated sphere to sediment a distance of one radius a, ρ_p and ρ_f are the particle and fluid densities, respectively, and η_0 is the fluid viscosity, which is constant since second-order fluids do not exhibit shear-thinning. The solution is obtained by applying a perturbation analysis, and then using Stokesian dynamics to solve the zero-order problem and the Reciprocal theorem method mentioned above to solve the first-order problem. Note that, because the second-order fluid model is only valid for small Deborah numbers, using a perturbation analysis does not impose any new restrictions

on the validity of the solution. In addition, since most well-known constitutive models reduce to the second-order fluid model for small Deborah numbers, that model should be sufficient for calculating sphere velocities to $O(De)$, thereby providing qualitative insight into changes due to the presence of elasticity.

Following Bird *et al.* (1987), we express the stress in the fluid $\boldsymbol{\tau}$ in terms of the retarded motion expansion, which to terms of second order yields

$$\boldsymbol{\tau} = -[\eta \boldsymbol{\gamma}_{(1)} + b_2 \boldsymbol{\gamma}_{(2)} + b_{11} \boldsymbol{\gamma}_{(1)} \cdot \boldsymbol{\gamma}_{(1)}], \tag{2}$$

with the rate-of-strain tensors defined by

$$\boldsymbol{\gamma}_{(1)} = \nabla \boldsymbol{u} + \nabla \boldsymbol{u}^t \tag{3}$$

and

$$\boldsymbol{\gamma}_{(2)} = \frac{\mathrm{D}}{\mathrm{D}t} \boldsymbol{\gamma}_{(1)} - [(\nabla \boldsymbol{u})^t \cdot \boldsymbol{\gamma}_{(1)} + \boldsymbol{\gamma}_{(1)} \cdot \nabla \boldsymbol{u}], \tag{4}$$

where $\boldsymbol{u}$ is the fluid velocity. In terms of the first and second normal stress differences Ψ_1 and Ψ_2, the coefficients b_2 and b_{11} are given by

$$b_2 = -\tfrac{1}{2}\Psi_1 \tag{5}$$

and

$$b_{11} = \Psi_2. \tag{6}$$

To non-dimensionalize the equations of motion, we define κ as a characteristic shear rate and use as a characteristic length the sphere radius a. For sedimentation, the shear rate κ is just $1/\tau_s$(cf. (1)). The Deborah number, defined as a ratio of characteristic times for the fluid and the flow field, respectively, is obtained by identifying $1/\kappa$ as a time scale for the flow and $-b_2/\eta$ as that for the fluid. The latter fluid time scale is consistent with that found from linear viscoelasticity models. Non-dimensionalizing the rate-of-strain tensors in (2) with λ then gives

$$\hat{\boldsymbol{\tau}} = -\hat{\boldsymbol{\gamma}}_{(1)} + De[\hat{\boldsymbol{\gamma}}_{(2)} + B_{11} \hat{\boldsymbol{\gamma}}_{(1)} \cdot \hat{\boldsymbol{\gamma}}_{(1)}], \tag{7}$$

where the dimensionless coefficient B_{11} is given by $B_{11} = b_{11}/b_2$ and the stress $\hat{\boldsymbol{\tau}} = \boldsymbol{\tau}/\eta\kappa$.

Assuming that inertial effects are negligible, the equations of motion and continuity can be expressed as

$$-\hat{\nabla}\hat{p} + \hat{\nabla} \cdot \hat{\boldsymbol{\tau}} = 0 \tag{8}$$

and

$$\hat{\nabla} \cdot \hat{\boldsymbol{u}} = 0. \tag{9}$$

We now introduce a perturbation expansion in powers of De, which is taken to be small, according to

$$\hat{\boldsymbol{u}} = \hat{\boldsymbol{u}}_0 + De\,\hat{\boldsymbol{u}}_1 \tag{10}$$

and

$$\hat{p} = \hat{p}_0 + De\,\hat{p}_1, \tag{11}$$

where $\hat{\boldsymbol{u}} = \boldsymbol{u}/a\kappa$ and $\hat{p} = p/\eta\kappa$. Substituting into (8) and (9) yields as the zero- and first-order problems:

zero order

$$\hat{\nabla} \cdot \hat{\boldsymbol{\Pi}}_0 = 0, \tag{12}$$

$$\hat{\nabla} \cdot \hat{\boldsymbol{u}}_0 = 0; \tag{13}$$

first order

$$\hat{\nabla} \cdot \hat{\boldsymbol{\Pi}}_1 = 0, \tag{14}$$

$$\hat{\nabla} \cdot \hat{\boldsymbol{u}}_1 = 0. \tag{15}$$

The zero- and first-order stresses in (12) and (13) include the pressure, and are given by

$$\hat{\boldsymbol{\Pi}}_0 = -\hat{p}_0 \boldsymbol{I} + \hat{\boldsymbol{\gamma}}_{(1)0} \tag{16}$$

and $$\hat{\boldsymbol{\Pi}}_1 = -\hat{p}_1 \boldsymbol{I} + \hat{\gamma}_{(1)1} - [\hat{\gamma}_{(2)0} + B_{11}\, \hat{\gamma}_{(1)0} \cdot \hat{\gamma}_{(1)0}], \tag{17}$$

where $\boldsymbol{I}$ is the identity tensor and the rate-of-strain tensors are non-dimensionalized using appropriate powers of the characteristic shear rate κ. Thus, the zero-order result is the solution to the Stokes flow problem, while the first-order equations resemble Stokes equations but have a non-homogeneous term that depends nonlinearly on the zero-order velocity field.

3. Method of solution

3.1. *Zero-order solution*

Because the zero-order problem is identical to a Stokes flow problem, any of a number of approaches could be used to obtain a solution. Here the Stokesian dynamics method is used because it has been shown to give accurate results for spheres in arbitrary locations and because it is readily applied to dynamic simulations (Durlofsky *et al.* 1987; Brady *et al.* 1988; Phillips, Brady & Bossis 1988*a*, *b*). The one exception is the problem of two spheres sedimenting along their line of centres, which we solve using both Stokesian dynamics and the method of reflections for purposes of comparison.

The details of Stokesian dynamics are described elsewhere (Durlofsky *et al.* 1987; Brady & Bossis 1988), and so only some key elements are summarized here. In this method, sphere interactions are separated into far-field and near-field components. Far-field perturbations to the fluid velocity caused by the particles are calculated by using a multipole moment expansion, which is used in conjunction with Faxén's laws to relate the perturbations in the fluid velocity to the corresponding perturbations in sphere velocities. Near-field, or lubrication interactions are incorporated into the resistance matrix by using a pairwise additivity approximation. For nearly touching particles in relative motion, this method of computing near-field interactions yields quantitatively accurate results. For spheres that are not in relative motion, such as those modelling constituents of a porous medium, lubrication forces are not important and the accuracy of the method is limited by the number of terms kept in the far-field multipole moment expansion (Phillips *et al.* 1988*a*, *b*). As commonly used, Stokesian dynamics does not require that one calculate the fluid velocity since the use of Faxén's laws allows one to compute the sphere velocities directly. In other words, the forces, torques and stresslets on the spherical particles are related directly to their translational and rotational velocities without explicit calculation of the fluid velocity.

For spheres in a quiescent fluid, this relationship is represented by a matrix equation of the form

$$\begin{bmatrix} \hat{\boldsymbol{F}}_{3N} \\ \hat{\boldsymbol{L}}_{3N} \\ \hat{\boldsymbol{S}}_{5N} \end{bmatrix} = \begin{bmatrix} \boldsymbol{R}_{FU} & \boldsymbol{R}_{F\Omega} & \boldsymbol{R}_{FE} \\ \boldsymbol{R}_{LU} & \boldsymbol{R}_{L\Omega} & \boldsymbol{R}_{LE} \\ \boldsymbol{R}_{SU} & \boldsymbol{R}_{S\Omega} & \boldsymbol{R}_{SE} \end{bmatrix} \cdot \begin{bmatrix} \hat{\boldsymbol{U}}_{3N} \\ \hat{\boldsymbol{\Omega}}_{3N} \\ 0 \end{bmatrix}. \tag{18}$$

The subscripts on the vector quantities refer to the dimension of the vector: $\hat{\boldsymbol{F}}_{3N}$ is a vector containing the three elements of the force vectors for each of the N particles, and so on. The matrix relating the two vectors is the *grand resistance matrix*, and is composed of smaller matrices that relate forces to translational velocities ($\boldsymbol{R}_{FU}$), forces to rotational velocities ($\boldsymbol{R}_{F\Omega}$), and so forth. It should be noted that the grand resistance matrix depends only on the sphere positions, and is independent of what particular combination of forces and torques is being applied to the spheres.

As stated above, the Reciprocal theorem method that is used here to solve the first-order problem *does* require the zero-order solution for the fluid velocity, and not just

a result for motion of the spheres as given in (18). This fluid velocity field can be obtained by going back to the multipole moment expansion that is an intermediate step in the Stokesian dynamics method, and reconstructing the velocity according to

$$u_i(\boldsymbol{x}) = \frac{1}{8\pi\eta}\sum_{\alpha}\left(1+\frac{a^2}{6}\nabla^2\right)J_{ij}F_j^{\alpha}+R_{ij}L_j^{\alpha}+\left(1+\frac{a^2}{10}\right)K_{ijk}S_{jk}^{\alpha}. \tag{19}$$

Here $\boldsymbol{F}$, L and $\boldsymbol{S}$ are the forces, torques and stresslets on the particles, $\boldsymbol{J}$ is the Oseen tensor, and $\boldsymbol{R}$ and $\boldsymbol{K}$ are propagators defined in terms of gradients of the Oseen tensor. A mathematical development of (19) and formal definitions of the moments $\boldsymbol{F}$, $\boldsymbol{L}$ and $\boldsymbol{S}$ and the propagators $\boldsymbol{J}$, $\boldsymbol{R}$ and $\boldsymbol{K}$ are given by Durlofsky *et al.* (1987). The superscript α is a sphere label that varies from 1 to N. Once the forces, torques and stresslets are known, either by being specified as part of the problem or by being calculated from (18), the velocity field valid in the far-field limit can be found directly from (19). For the problem of N sedimenting spheres considered here, the forces are non-zero and are specified as the gravitational force, and the torques are zero. Therefore, only the stresslets must be calculated from (18).

3.2. *First-order solution*

The solution to first order is obtained by using the Reciprocal theorem method alluded to above. We begin by defining an *auxiliary* Stokes flow problem. In the auxiliary problem, N identical spheres with radius a are suspended in a Newtonian fluid in the same positions as in the original problem. Either the forces and torques or the translational and rotational velocities may be specified in a manner that is most convenient for a particular problem. Specific choices for the problem at hand are discussed below. We denote the velocity and pressure for the new problem as $\boldsymbol{v}$ and q, and the stress by $\boldsymbol{\sigma}$. The governing equations are then

$$\hat{\nabla}\cdot\hat{\boldsymbol{\sigma}} = 0 \tag{20}$$

and

$$\hat{\nabla}\cdot\hat{\boldsymbol{v}} = 0, \tag{21}$$

where

$$\hat{\boldsymbol{\sigma}} = -\hat{q}\boldsymbol{I}+\hat{\boldsymbol{e}} \tag{22}$$

and $\hat{\boldsymbol{e}}$ is the rate of strain given by $\hat{\boldsymbol{e}} = \nabla\hat{\boldsymbol{v}}+\nabla\hat{\boldsymbol{v}}^t$. Note that the grand resistance matrix for this new problem is identical to that for the zero-order solution to the original problem, since the resistance matrix only depends on the sphere positions.

From equations (14) and (20), it must be true that

$$\int_{V_f}[\hat{\boldsymbol{v}}\cdot(\hat{\nabla}\cdot\hat{\boldsymbol{\Pi}}_1)-\hat{\boldsymbol{u}}_1\cdot(\hat{\nabla}\cdot\hat{\boldsymbol{\sigma}})]\,\mathrm{d}V = 0, \tag{23}$$

where V_f is the fluid volume and does not include the spheres. Rearranging (23) gives

$$\int_{V_f}\hat{\nabla}\cdot[\hat{\boldsymbol{v}}\cdot\hat{\boldsymbol{\Pi}}_1-\hat{\boldsymbol{u}}_1\cdot\hat{\boldsymbol{\sigma}}]\,\mathrm{d}V-\int_{V_f}[\hat{\boldsymbol{\Pi}}_1:\hat{\nabla}\hat{\boldsymbol{v}}-\hat{\boldsymbol{\sigma}}:\nabla\hat{\boldsymbol{u}}_1]\,\mathrm{d}V = 0. \tag{24}$$

Applying the divergence theorem to the first integral in (24) and substituting the definitions from (17) and (22) into the second yields

$$\sum_{\alpha}\int_{S_{\alpha}}\boldsymbol{n}\cdot(\hat{\boldsymbol{v}}\cdot\hat{\boldsymbol{\Pi}}_1-\hat{\boldsymbol{u}}_1\cdot\hat{\boldsymbol{\sigma}})\,\mathrm{d}S = \int_{V_f}[(\hat{\gamma}_{(2)0}+B_{11}\hat{\gamma}_{(1)0}\cdot\hat{\gamma}_{(1)0}):\hat{\nabla}\hat{\boldsymbol{v}}]\,\mathrm{d}V, \tag{25}$$

where the continuity equations (15) and (21) have been used to simplify terms.

We now make use of the fact that, on sphere surfaces, the velocity $\hat{\boldsymbol{v}}$ and the perturbation velocity $\hat{\boldsymbol{u}}_1$ are constrained by the no-slip condition to be a superposition of translational and rotational sphere motion. Also, the $O(De)$ forces and torques

(surface integrals of $\hat{\boldsymbol{\Pi}}_1$) must be zero since the applied torques are zero and the applied forces are completely accounted for in the zero-order problem. Making the appropriate substitutions into the surface integral in (25) then gives

$$\sum_{\alpha} \hat{\boldsymbol{U}}_1^{\alpha} \cdot \hat{\boldsymbol{F}}_v^{\alpha} + \hat{\boldsymbol{\Omega}}_1^{\alpha} \cdot \hat{\boldsymbol{L}}_v^{\alpha} = \int_{V_f} [(\hat{\gamma}_{(2)0} + \boldsymbol{B}_{11}\, \hat{\gamma}_{(1)0} \cdot \hat{\gamma}_{(1)0}) : \hat{\boldsymbol{\nabla}} \hat{\boldsymbol{v}}] \, \mathrm{d}V. \tag{26}$$

Here $\hat{\boldsymbol{U}}_1^{\alpha}$ and $\hat{\boldsymbol{\Omega}}_1^{\alpha}$ are the desired $O(De)$ perturbation velocities and $\hat{\boldsymbol{F}}_v^{\alpha}$ and $\hat{\boldsymbol{L}}_v^{\alpha}$ are the applied force and torque in the auxiliary problem. Appropriate choices for $\hat{\boldsymbol{F}}_v^{\alpha}$ and $\hat{\boldsymbol{L}}_v^{\alpha}$ allow one to calculate the velocity corrections using only solutions to Stokes flow problems.

As an example which shall be of use below, for our auxiliary problem we choose the forces and torques on all the particles to be zero, with the exception of particle β, which has a non-zero force $\hat{\boldsymbol{F}}_v^{\beta}$. Equation (26) then simplifies to

$$\hat{\boldsymbol{U}}_1^{\beta} \cdot \hat{\boldsymbol{F}}_v^{\beta} = \int_{V_f} [(\hat{\gamma}_{(2)0} + B_{11}\, \hat{\gamma}_{(1)0} \cdot \hat{\gamma}_{(1)0}) : \hat{\boldsymbol{\nabla}} \hat{\boldsymbol{v}}] \, \mathrm{d}V. \tag{27}$$

Equation (27) provides a means for calculating the $O(De)$ corrections to the three components of the zero-order sphere velocities. Choosing $\hat{\boldsymbol{F}}_v^{\beta}$ equal to a unit vector in the x-direction and substituting the appropriate velocity field into the volume integral yields $\hat{U}_{1x}^{\alpha}$, and the y and z components are calculated similarly. Evaluation of the integral requires only the Newtonian velocity profiles, which can be found by a multipole expansion such as (19) or by other techniques such as the method of reflections, as discussed in §4.

For incorporation of this method into Stokesian-dynamics-like simulations of the motions of N spheres, it is convenient to choose an alternative auxiliary problem which corresponds to a 'resistance' formulation, in which particle velocities are specified rather than applied forces and torques. We specify either the translational or rotational velocity of sphere β of the auxiliary problem to be non-zero, while specifying that all other translational and rotational velocities be zero. The forces and torques $\hat{\boldsymbol{F}}_v^{\alpha}$ and $\hat{\boldsymbol{L}}_v^{\alpha}$ in (26) can be calculated from the resistance matrix as shown in (18). If the dimensionless translational and rotational velocities of the auxiliary problem are chosen to be unit vectors in the three coordinate directions, then substitution of the result for $\hat{\boldsymbol{F}}_v^{\alpha}$ and $\hat{\boldsymbol{L}}_v^{\alpha}$ into (26) yields a set of linear equations of the form

$$\begin{bmatrix} \boldsymbol{R}_{FU} & \boldsymbol{R}_{F\Omega} \\ \boldsymbol{R}_{LU} & \boldsymbol{R}_{L\Omega} \end{bmatrix} \cdot \begin{bmatrix} \hat{\boldsymbol{U}}_{1,3N} \\ \hat{\boldsymbol{\Omega}}_{1,3N} \end{bmatrix} = \int_{V_f} [(\hat{\gamma}_{(2)0} + \boldsymbol{B}_{11}\, \hat{\gamma}_{(1)0} \cdot \hat{\gamma}_{(1)0}) : \hat{\boldsymbol{\nabla}} \hat{\boldsymbol{v}}_{6N}] \, \mathrm{d}V. \tag{28}$$

Here $\hat{\boldsymbol{v}}_{6N}$ is the velocity vector obtained by setting each component of translational or rotational velocity equal to unity for each sphere while keeping all other velocity components equal to zero. One sees that, owing to the use of the perturbation expansion in De, the nonlinearity in the original problem now occurs only in the known terms on the right-hand side. Multiplication of (28) by the Deborah number De and adding it to the zero-order equation (18) then yields a single matrix equation for the particle velocities accurate to $O(De)$. In effect, the volume integral in (28) acts as a correction to the applied forces that, once calculated, can be incorporated directly into the Stokesian dynamics simulation.

3.3. *Surface integral formulation*

Implementation of (27) or (28) for simulating particle motion at low Deborah number is made considerably more efficient by expressing the volume integral as a surface integral. This simplification can be made if one assumes a value of unity for the

parameter B_{11}. We note that realistic values are likely to be closer to 0.5 or smaller (Bird *et al.* 1987). However, the factor of two difference is not expected to alter significantly the qualitative changes in behaviour of interest here, an assumption that is supported by results for the two-sphere problem discussed below. In the development that follows we drop the $\hat{}$ notation, with the understanding that all quantities in this section are dimensionless.

Letting $B_{11} = 1$, we have for the integrand of (26)

$$(\gamma_{(2)0}+\gamma_{(1)0}\cdot\gamma_{(1)0}):\nabla v = \nabla\cdot[(\gamma_{(2)0}+\gamma_{(1)0}\cdot\gamma_{(1)0})\cdot v]-[\nabla\cdot(\gamma_{(2)0}+\gamma_{(1)0}\cdot\gamma_{(1)0})]\cdot v. \quad (29)$$

We now make use of Giesekus' identity (Bird *et al.* 1987), which states that

$$\nabla\cdot(\gamma_{(2)0}+\gamma_{(1)0}\cdot\gamma_{(1)0}) = \nabla\left[\frac{Dp_0}{Dt}+\tfrac{1}{4}(\gamma_{(1)0}:\gamma_{(1)0})\right]. \quad (30)$$

Substituting into (29) and noting that $\nabla\cdot v = 0$, we find for the integrand

$$\nabla\cdot\left\{(\gamma_{(2)0}+\gamma_{(1)0}\cdot\gamma_{(1)0})\cdot v-v\left[\frac{Dp_0}{Dt}+\tfrac{1}{4}(\gamma_{(1)0}:\gamma_{(1)0})\right]\right\}. \quad (31)$$

Application of the divergence theorem then yields

$$\sum_\alpha \hat{U}_1^\alpha\cdot\hat{F}_v^\alpha+\hat{\Omega}_1^\alpha\cdot\hat{L}_v^\alpha = \sum_\alpha\int_{S_\alpha}\left\{(\gamma_{(2)0}+\gamma_{(1)0}\cdot\gamma_{(1)0}):vn-(n\cdot v)\left[\frac{Dp_0}{Dt}+\tfrac{1}{4}(\gamma_{(1)0}:\gamma_{(1)0})\right]\right\}dS. \quad (32)$$

Equation (32) is a scalar equation that must be applied six times, corresponding to six different auxiliary problems, to calculate the $O(De)$ perturbation to the translational and rotational velocity of a given particle. We note that, when using the auxiliary problem in which one particle is translating or rotating and all others are stationary, the summation over all particle surfaces is not necessary since the velocity v will be non-zero only on one surface. In addition, as with (26), the left-hand side can be written in matrix form and the right-hand side as a $6N$-dimensional vector to represent the $6N$ linear equations, which are then easily combined with (18).

Further manipulation of the surface integral in (32) is useful for evaluating the time derivative $\partial p_0/\partial t$ that is part of the material derivative term Dp_0/Dt and the time derivative $\partial\gamma_{(1)0}/\partial t$ that comprises part of $\gamma_{(2)0}$ (cf. (4)). We first impose the no-slip condition on the particle surfaces, so that

$$v = V+W\times r^\alpha, \quad (33)$$

where V and W are the translational and rotational velocities imposed through the auxiliary problem (i.e. unit vectors) and $r^\alpha = r-r_0^\alpha$, where r_0^α is the position of the centre of sphere α.

Upon substitution of (33) into (32), the surface integral can be separated into two parts, one proportional to V and the other to W. The time derivatives in the term proportional to V are

$$V\cdot\int_{S_\alpha}\left(-\frac{\partial\gamma_{(1)0}}{\partial t}+\frac{\partial p_0}{\partial t}I\right)\cdot n\,dS = V\cdot\frac{\partial F^\alpha}{\partial t}, \quad (34)$$

where F^α is the externally applied force on particle α. In equating the two terms in (34) we have used the definition of the zero-order stress Π_0 given in (16). Also, following Brunn (1977*a*, *b*), we have denoted S_α as a space-fixed surface which momentarily

coincides with the particle surface. The time derivatives in the term proportional to $\boldsymbol{W}$ are

$$\boldsymbol{W}\cdot\int_{S_\alpha}\left[-\boldsymbol{r}^\alpha\times\left(\frac{\partial\boldsymbol{\gamma}_{(1)0}}{\partial t}\cdot\boldsymbol{n}\right)+\frac{\partial\rho_0}{\partial t}\boldsymbol{r}^\alpha\times\boldsymbol{n}\right]\mathrm{d}S=\boldsymbol{W}\cdot\int_{S_\alpha}\left[-\boldsymbol{r}^\alpha\times\frac{\partial}{\partial t}(\boldsymbol{\Pi}_0\cdot\boldsymbol{n})\right]\mathrm{d}S. \tag{35}$$

By using the fact that $\partial\boldsymbol{r}^\alpha/\partial t=-\boldsymbol{U}_0^\alpha$, it is straightforward to show that the right-hand side of (35) simplifies to

$$\boldsymbol{W}\cdot\left(\frac{\partial\boldsymbol{L}^\alpha}{\partial t}+\boldsymbol{U}_0^\alpha\times\boldsymbol{F}^\alpha\right). \tag{36}$$

The surface integral form of (28) (valid when $B_{11}=1$) can now be written and added to the zero-order matrix equation (15) to yield a Stokesian-dynamics-like simulation method that accounts for leading-order effects of viscoelasticity. The result is

$$\begin{bmatrix}\boldsymbol{R}_{FU} & \boldsymbol{R}_{F\Omega}\\ \boldsymbol{R}_{LU} & \boldsymbol{R}_{L\Omega}\end{bmatrix}\cdot\begin{bmatrix}\boldsymbol{U}_{3N}\\ \boldsymbol{\Omega}_{3N}\end{bmatrix}=\begin{bmatrix}\boldsymbol{F}_{3N}+De\,\boldsymbol{F}'_{3N}\\ \boldsymbol{L}_{3N}+De\,\boldsymbol{L}'_{3N}\end{bmatrix}. \tag{37}$$

The translational and rotational velocities in (37) are accurate to $O(De)$. Each three-component vector of the correction forces and torques $\boldsymbol{F}'_{3N}$ and $\boldsymbol{L}'_{3N}$ is given by

$$\boldsymbol{F}'^\alpha=\frac{\partial\boldsymbol{F}^\alpha}{\partial t}+\int_{S_\alpha}\{-(\boldsymbol{u}_0\cdot\nabla\boldsymbol{\gamma}_{(1)0}-\nabla\boldsymbol{u}_0^t\cdot\boldsymbol{\gamma}_{(1)0}-\boldsymbol{\gamma}_{(1)0}\cdot\nabla\boldsymbol{u}_0+\boldsymbol{\gamma}_{(1)0}\cdot\boldsymbol{\gamma}_{(1)0})\cdot\boldsymbol{n}$$
$$+(\boldsymbol{u}_0\cdot\nabla p_0+\tfrac{1}{4}\boldsymbol{\gamma}_{(1)0}:\boldsymbol{\gamma}_{(1)0})\boldsymbol{n}\}\,\mathrm{d}S \tag{38}$$

and

$$\boldsymbol{L}'^\alpha=\frac{\partial\boldsymbol{L}^\alpha}{\partial t}+\boldsymbol{U}_0^\alpha\times\boldsymbol{F}^\alpha-\int_{S_\alpha}\boldsymbol{r}^\alpha\times[(\boldsymbol{u}_0\cdot\nabla\boldsymbol{\gamma}_{(1)0}-\nabla\boldsymbol{u}_0^t\cdot\boldsymbol{\gamma}_{(1)0}-\boldsymbol{\gamma}_{(1)0}\cdot\nabla\boldsymbol{u}_0+\boldsymbol{\gamma}_{(1)0}\cdot\boldsymbol{\gamma}_{(1)0})\cdot\boldsymbol{n}]\,\mathrm{d}S. \tag{39}$$

We note that (38) and (39) are consistent with the single-particle result of Brunn (1977*a*), which was verified for ellipsoidal particles by Kim (1986). In the sedimentation problem to be considered in the next section, both time derivatives in (38) and (39) are zero. The $\boldsymbol{U}_0^\alpha\times\boldsymbol{F}^\alpha$ term in (39) is zero for a single sphere in an unbounded fluid, but is in general non-zero for non-spherical particles and for systems with two or more spherical particles.

As a final point, we note that even in conditions where the global or average Deborah number is small, it is possible that in a particular region of fluid, such as between two particles in relative motion, the local Deborah number may not be small. Thus, the error due to the use of a perturbation expansion in De could compound the error caused by the use of a far-field approximation to the fluid velocity when calculating the interaction between nearly touching spheres. The calculations below are therefore restricted to dilute systems, and it is assumed that the qualitative behaviour of interest is not significantly affected by these limitations when spheres are close together. Comparisons with experimental observations tend to support this assumption.

4. Results and discussion

In this section, the development above is used to calculate the $O(De)$ correction to sphere velocities for problems involving two- and multi-sphere interactions. Two-sphere results are calculated by evaluating the volume integral in (27), while the many-

sphere results are obtained by application of (37). Previous results are available in the literature for the one-sphere problem (Brunn 1976), and also the two-sphere problem, providing the sphere separation is large (Brunn 1977*b*). To the best of our knowledge, solutions to problems involving interactions between more than two particles in second-order fluids are not available in the literature. However, it is interesting to recompute the Stokesian dynamics calculations of Durlofsky *et al.* (1987) to observe the leading-order effects of viscoelasticity. These results and results from simulations of the sedimentation of unbounded suspensions are also compared qualitatively with experimental observations (Allen & Uhlherr 1989; Joseph *et al.* 1992, 1994).

4.1. *The interaction between two spheres*

Once one moves from a one-sphere to a two-sphere problem, hydrodynamic interactions become important and must be taken into account in some fashion. The problem of two spheres sedimenting parallel or perpendicular to their line-of-centres is analysed here, while results of dynamic simulations involving more than two spheres are presented in §4.2. Two approaches are used to calculate the integral in (27): Stokesian dynamics in conjunction with the multipole moment expansion (19), and the method of reflections. For both problems, the $O(De)$ contribution to sphere motion moves the spheres together along their line-of-centres, with other components of $\hat{\boldsymbol{U}}_1$ being zero. The results are presented in terms of two coefficients, C_1 and C_2, which are defined by

$$\hat{U}_1^{\alpha} = (-1)^{\alpha+1}(C_1 + B_{11}\, C_2), \tag{40}$$

where $\hat{U}_1^{\alpha}$ is the component of $\hat{\boldsymbol{U}}_1$ along the line-of-centres and α can be 1 or 2. Comparison with (27) shows that C_1 can be expressed as a volume integral of $\hat{\gamma}_{(2)0}$, while C_2 can be expressed as a volume integral of $\hat{\gamma}_{(1)0} \cdot \hat{\gamma}_{(1)0}$. The factor $(-1)^{\alpha+1}$ accounts for the fact that, in two-sphere problems, symmetry results in the $O(De)$ perturbation in one sphere's velocity being equal to the negative of the perturbation to the other sphere's velocity.

Multiple moment expansion

We begin with the problem of two spheres sedimenting along their line-of-centres. Spheres 1 and 2 are located at $x = 0$ and $y = \frac{1}{2}l$ and $-\frac{1}{2}l$, respectively. Both spheres are subject to a unit force in the $-\boldsymbol{e}_y$ direction. As our auxiliary Stokes flow problem defined in terms of the velocity and pressure $\hat{\boldsymbol{v}}$ and $\hat{q}$, we choose two spheres at the same position, but we let the sphere at $y = -\frac{1}{2}l$ be force-free while the sphere at $y = \frac{1}{2}l$ is acted upon by a force equal to $\boldsymbol{e}_x$, $\boldsymbol{e}_y$ or $\boldsymbol{e}_z$. Choosing the force in either the $\boldsymbol{e}_x$ or $\boldsymbol{e}_z$ directions verifies the result stated above that the $O(De)$ perturbation is only non-zero in the direction along the line-of-centres, which in this case is the $\boldsymbol{e}_y$ direction. Choosing the force in the $\boldsymbol{e}_y$ direction then allows one to calculate C_1 and C_2 from (27).

The procedure is as follows. The force on each sphere is known both for the actual problem and for the auxiliary problem. Thus, the Newtonian sphere velocities are found by solving the matrix equation (18). The grand resistance matrix in (18), which is obtained by the Stokesian dynamics method, is exact for two-sphere problems. With the sphere velocities known, the stresslet $\hat{\boldsymbol{S}}^2$ induced on sphere 2 (at $y = -\frac{1}{2}l$) due to the force applied to sphere 1 (at $y = \frac{1}{2}l$) can be found by straightforward matrix multiplication, again using (18). Finally, the velocities and velocity gradients needed to compute the integral in (27) are found by making use of (19). The contribution from each sphere is calculated from the leading-order term (force, torque or stresslet) in (19), and the integration is performed in bipolar coordinates.

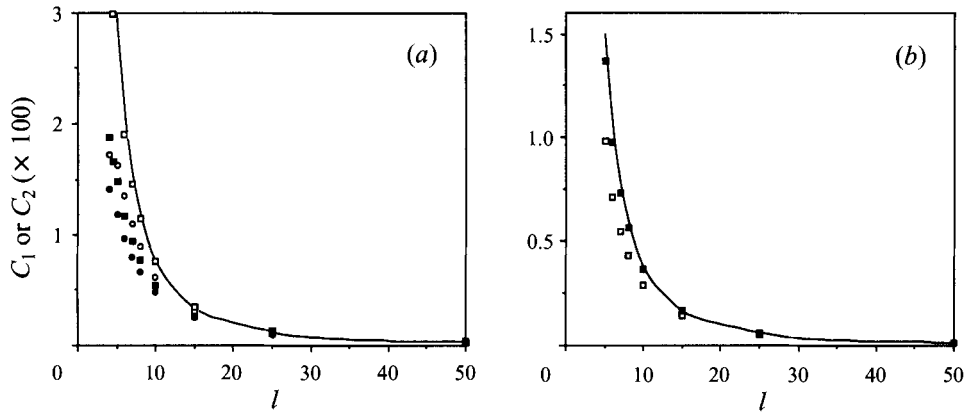

FIGURE 1. Coefficients C_1 and C_2 defined in (40) are plotted as a function of sphere position l for two spheres sedimenting (*a*) along their line of centres and (*b*) perpendicular to their line-of-centres. Solid curve is the asymptotic result of Brunn (1977*b*). Squares are the results obtained by using the multipole moment expansion, and circles in (*a*) are results from the method of reflections. Open symbols are C_1 and closed symbols are C_2.

The results for C_1 and C_2 are shown in figure 1. Both coefficients are positive for all values of l, indicating that the effect of elasticity in the fluid is to speed up the upper sphere and slow down the lower sphere. This of course causes the two spheres to move together, in contrast to the Newtonian case where the separation remains constant. The fact that both C_1 and C_2 increase as the separation l decreases means that the spheres move together increasingly faster as they come together. Also shown is the result of Brunn (1977*b*), who predicted that the two coefficients are equal in the far-field limit and that they are given by

$$C_1 = C_2 = \tfrac{3}{4}(1/l)^2. \tag{41}$$

Clearly Brunn's result is in excellent agreement with those found from (27) when l is greater than about 15.

For comparison, the velocity field for two spheres moving along their line-of-centres has also been calculated by using the method of reflections. These calculations were performed by using the solution reported by Happel & Brenner (1986) and incorporates terms from the first five reflections. Gradients of the velocity field were evaluated by direct term-by-term differentiation, and again the volume integral of (27) was evaluated in bipolar coordinates. The results, shown in figure 1, confirm both the asymptotic solution of Brunn (1977*b*) and the results obtained by using the multipole moment expansion. Finally, we note that if one assigns a value of unity to the coefficient B_{11}, then the sum $C_1 + C_2$ can be calculated via the surface integral formulation and (37), and one again finds similarly good agreement. This latter calculation is verification of the computer programs used to obtain the results, since both the auxiliary problems used in the derivations of (27) and (37) and the detailed computation for the two cases are quite different.

The prediction of the second-order fluid constitutive model that two sedimenting spheres always move together is in apparent contradiction with the observations of Riddle *et al.* (1977), who found that two spheres in a tube move apart if the initial separation is large. This separation behaviour is often explained in terms of the negative wake that is present when particles sediment in viscoelastic fluids (Bisgaard 1983). The fact that two spheres in a second-order fluid move together may therefore

suggest that this model does not accurately capture the negative wake effect, a characteristic which is also true of the convected Maxwell model (Satrape & Crochet 1994). It has also been suggested (McKinley, Armstrong & Brown 1993) that the negative wake is closely connected with shear-thinning, a rheological feature that is not captured here.

The case of two spheres sedimenting in a direction perpendicular to their line-of-centres is handled in an analogous fashion. Spheres 1 and 2 are at $x = -\frac{1}{2}l$ and $x = \frac{1}{2}l$, respectively, and both are subject to a unit force in the $-\boldsymbol{e}_y$ direction. Results for C_1 and C_2 obtained by using the multipole moment expansion are plotted as a function of the separation l in figure 1(*b*). Again, both coefficients are positive, indicating that the spheres move together at a rate that increases with decreasing l. This motion is qualitatively different than that observed in a Newtonian fluid, where the principle of reversibility requires that the sphere separation remain constant. The result of Brunn (1977*b*), given by

$$C_1 = C_2 = \tfrac{3}{8}(1/l)^2 \tag{42}$$

is also shown in figure 1(*b*) for comparison. As with the case of spheres moving parallel to their line-of-centres, agreement is excellent in the far-field limit.

4.2. *Dynamic simulations at low Deborah number*

We now consider the case where the coefficient B_{11} is unity, allowing use of the surface formulation of the problem as given by (37). The result in (40) for the motion of two spheres, together with the far-field solutions for C_1 and C_2 given by (41) and (42) (and in figure 1), show that C_1 and C_2 behave similarly, and hence the qualitative effects of elasticity are not changed by assuming a particular value of B_{11}. Although in a simulation the effect of elasticity on particle motion is very small for each individual time step, as shown below the cumulative impact over many time steps can be quite dramatic, and can completely alter the qualitative nature of the solution. Unless otherwise indicated, the results shown in this section were computed using a Deborah number of $De = 0.1$. The time integrations were performed by using a fourth-order Runge–Kutta routine. The maximum dimensionless time step used was 0.25, where time is made dimensionless by τ_s, the time for a single sphere to sediment a distance of one radius a. The surface integrations were performed by applying Simpson's rule with 41 nodes.

We begin by reconsidering three- and four-sphere simulations initially performed by Stokesian dynamics (Durlofsky *et al.* 1987) for spheres in Newtonian fluids. We consider three spheres aligned in a row along the x-axis, located at $x = -5$, 0 and 7. The spheres are subject to a force of unity acting in the $-\boldsymbol{e}_y$ direction, and hence the sphere centres never leave the (x, y)-plane. The trajectories calculated by Stokesian dynamics are recomputed here for comparison, and are shown in figure 2(*a*). The spheres follow surprisingly varying paths, but after falling a distance of approximately 830 sphere radii they all have similar y positions. Each point in figure 2(*a*) and in the similar trajectories shown in figures 2(*b*), 4 and 6 below denote a change of 10 dimensionless time units.

The corresponding result for three spheres in a second-order fluid at a Deborah number of 0.1 is shown in figure 2(*b*). Because this result is an $O(De)$ perturbation from the Newtonian case, the sphere trajectories are initially very similar. However, the interaction between the sphere initially at $x = -5$ and that initially at $x = 7$ causes a dramatic change at a dimensionless time of approximately 200. Those two spheres ultimately form a doublet located at $x = 4.5$ and falling vertically, while what started

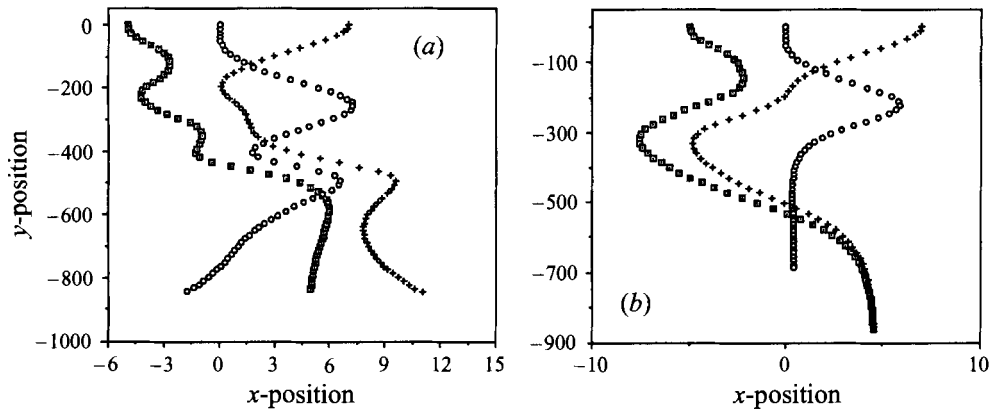

FIGURE 2. Trajectories of three spheres sedimenting in (*a*) a Newtonian fluid and (*b*) a second-order fluid at $De = 0.1$. Initial x-positions are -5, 0 and 7.

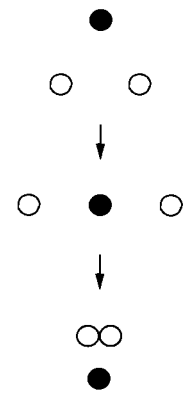

FIGURE 3. Schematic diagram of the sedimentation of three spheres initially at the vertices of an equilateral triangle.

out as the middle sphere is eventually located at $x = 0.44$. Because a doublet falls faster than a single sphere, the vertical distance between the spheres grows, reaching a value of 174 at a time of 600, and becoming increasingly larger after that time. We note that at this large separation the interaction between the single sphere and the doublet is negligible. Since an isolated sphere or two-sphere doublet in a second-order fluid falls with the same velocity as in a Newtonian fluid, the effects of elasticity are only significant in the initial stages of the simulation.

Interestingly, if one starts a three-sphere simulation from a more ordered configuration, the behaviour is considerably less erratic. Several simulations have been performed in which the spheres are initially at the corners of an equilateral triangle, the coordinates (x, y) of spheres 1, 2 and 3 being given by $(0,0)$, $(\frac{1}{2}l_t, \frac{1}{2}\sqrt{3}\,l_t)$ and $(l_t, 0)$, respectively. As discussed by Ganatos *et al.* (1978), in a Newtonian fluid, following application of a unit force in the $-\boldsymbol{e}_y$ direction, sphere 2 falls faster than the others until eventually all three spheres lie equally spaced in a row. This process is depicted in figure 3. Sphere 2 continues to fall the fastest, falling below spheres 1 and 3, which move together until the distance between them is infinitesimally small.

Very similar behaviour is observed in the simulations for a second-order fluid. However, there are some quantitative and qualitative differences. For example, for

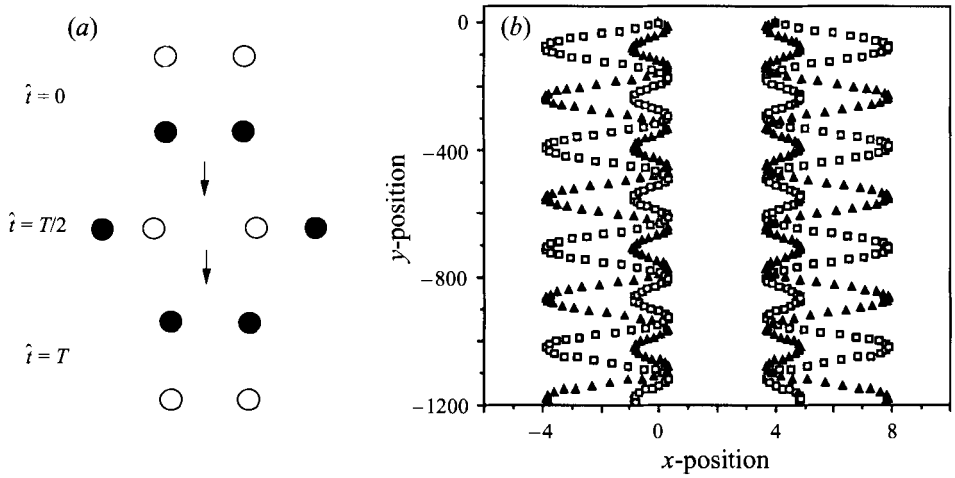

FIGURE 4. (*a*) Schematic diagram and (*b*) plotted trajectories of four spheres undergoing a periodic inversion process while sedimenting in a Newtonian fluid. Spheres are initially located at the vertices of a square.

$l_t = 8$ the time for the spheres to form a horizontal row is 105.0 for the Newtonian case and 100.3 in the second-order fluid, and the sphere separations in the row differ slightly, being 7.4 for the Newtonian case and 7.2 in the second-order fluid. Also, regardless of the value of the side length, in the second-order fluid the three spheres always evolve into the same configuration, with spheres 1 and 3 two radii apart and sphere 2 midway between and a distance of 2.82 below the others. Such a constant configuration is not possible in the Newtonian case, since it would violate the principle of reversibility. For example, for $l_t = 8$ the three spheres assume the final configuration shown in figure 3 for both the Newtonian and second-order cases. However, for the Newtonian simulation the vertical distance between spheres 1 and 3 and sphere 2 changes from 3.08 to 2.96 when the time changes from 380 to 430. In contrast, the separation in the second-order fluid remains constant at 2.82.

We next consider a simulation of four spheres located at the corners of a square with sides of length l_s, where the spheres are again sedimenting in the (x, y)-plane that contains the sphere centres. As discussed by Hocking (1964) and later simulated by Durlofsky *et al.* (1987), four spheres in such a configuration undergo a periodic inversion process. As shown in figure 4(*a*), initially this inversion consists of the upper two spheres catching up the lower two, forming a row in which the middle two spheres are separated by a distance greater than that separating either the left or right pairs of spheres. Subsequently, a square with side length l_s forms again, but with what were initially the upper spheres on the bottom and what were initially the lower spheres on top. This inversion process repeats itself periodically, forming trajectories such as those shown in figure 4(*b*), which were calculated by Stokesian dynamics for a sphere with sides that are four radii in length.

The introduction of a small amount of elasticity changes this qualitative behaviour in an interesting and dramatic way. Shown in figure 5 is the schematic diagram for trajectories in a second-order fluid at a Deborah number of 0.1 for a square with a side length l_s equal to six sphere radii. Comparing this diagram with that of figure 4(*a*), one sees that the inversion process in the non-Newtonian case begins as expected. However, during the sedimentation the left and right pairs of spheres get rather close together, and the effect of elasticity is to cause the two pairs to separate into doublets. The two

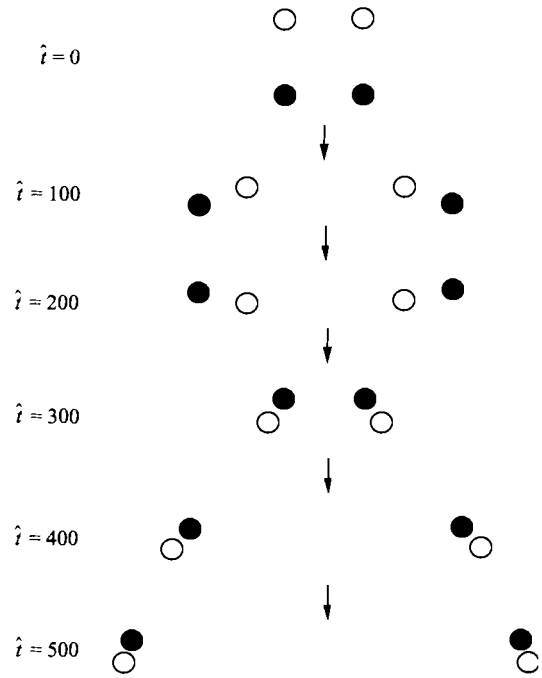

FIGURE 5. Schematic diagram of four spheres sedimenting in a second-order fluid at $De = 0.1$. Initial configuration is a square with a side length of six radii.

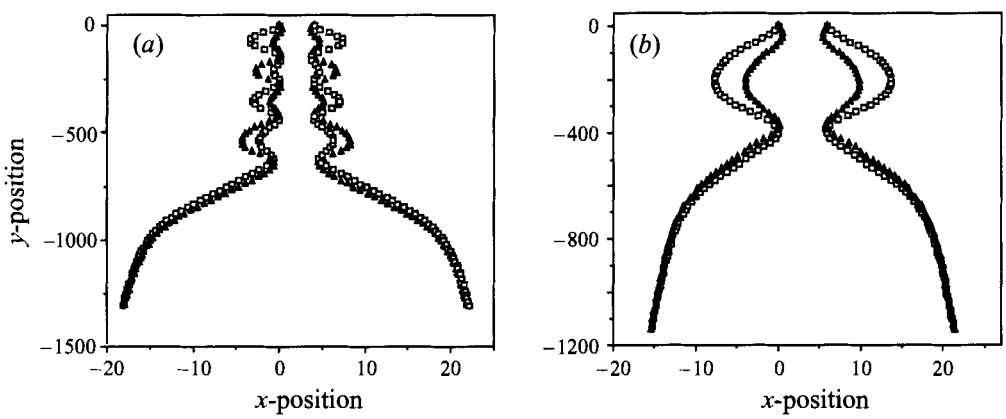

FIGURE 6. Trajectories of four spheres sedimenting in a second-order fluid at $De = 0.1$. Initial configurations are squares with side lengths of (*a*) four and (*b*) six radii.

doublets are oriented such that they would move away from each other even in a Newtonian fluid, with the $U \times F$ term of (39) causing each doublet to change its orientation such that the line-of-centres becomes parallel to the y-axis. This change in orientation is similar to that calculated by Kim (1986) for spheroidal particles.

An overview of the process is shown for squares with side lengths of 4 and 6 radii in figures 6(*a*) and 6(*b*), respectively. Comparing figures 6(*a*) and 4(*b*), one sees that there is an obvious similarity between the trajectories during the first half of the simulation. However, the cumulative effect of elasticity is to cause doublets to form and separate, as described above. The separation takes somewhat longer in the square with a side length of 4 radii than in that with a side length of 6 radii. In both cases the

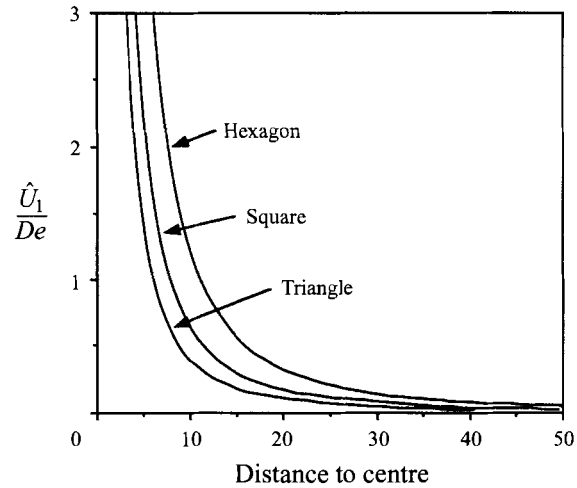

FIGURE 7. The leading-order coefficient $\hat{U}_1/De$ governing the rate at which spheres initially located at the vertices of regular polygons move together is plotted versus distance to the polygon centre. Spheres are subject to a force perpendicular to the plane containing the vertices.

doublets ultimately are far enough apart so that their interaction is negligible. Thus, like in the three-sphere simulation shown in figure 2(*b*), one effect of elasticity seems to be to cause the formation of chains of particles oriented in the direction of sedimentation. This qualitative behaviour is reminiscent of the structures observed by Joseph *et al.* (1992, 1994) during sedimentation in a viscoelastic fluid.

Although the simulations considered so far have involved situations in which all the sphere centres lie in the same plane, the method is of course equally applicable to fully three-dimensional problems, and indeed the simulation program explicitly includes the z-direction. As an example three-dimensional calculation, we consider problems with three, four and six spheres at the vertices of equilateral triangles, squares and hexagons with equal-sized sides. The spheres are subject to a force in the direction perpendicular to the plane containing the vertices of the polygon. Such a configuration is stable at zero Reynolds number. However, in the second-order fluid, in each case the spheres move towards the centre of the polygon. The coefficients $\hat{U}_1/De$ that, when multiplied by the Deborah number De give the sphere velocities in the direction of the line joining the sphere centre to the centre of the polygon, are plotted as a function of the distance to the polygon centre l_c in figure 7. In each case the velocity of the spheres increases with decreasing distance, with the magnitude always being largest for the configuration containing the greater number of spheres.

4.3. *Dynamic simulation of sedimenting suspensions*

The dramatic changes in the motion of small numbers of spheres caused by a small amount of elasticity are also evident in sedimenting suspensions. Experimental evidence for this effect can be found in the globular and finger-like structures observed by Allen & Uhlherr (1989) and in the clustering observations of Joseph *et al.* (1992, 1994). Some qualitative insight into the development of the non-homogeneous microstructure in suspensions sedimenting in viscoelastic fluids can be obtained by Stokesian dynamics simulation. As in previous work (Brady & Bossis 1988), we confine the spheres to a monolayer, and model the unbounded nature of the suspension by using periodic boundary conditions.

N	ϕ	De	Number of simulations
15	0.05	0.1	5
15	0.15	0.1	5
25	0.05	0.1	4
25	0.15	0.1	4
25	0.05	0.01	4
25	0.15	0.01	4

TABLE 1. Number of simulations at varying conditions.

A series of such simulations has been performed with the number of spheres N in each periodic unit cell equalling either 15 or 25. Sphere area fractions of $\phi = 0.05$ and 0.15 are considered, at Deborah numbers of 0.01 and 0.1. The number of simulations at each set of conditions is shown in table 1. Although 25 spheres is not expected to be enough to provide quantitative information, it is sufficient to obtain the qualitative information that one anticipates from a second-order fluid model. We note that 25-sphere simulations have been used to obtain quantitative information for monolayer simulations of sheared suspensions (Chang & Powell 1994). However, here we are limited to qualitative, microstructural information because of the more complicated nature of the sedimentation problem, in which particles are not force-free but are subject to an externally imposed gravitational force.

With the exception of the periodic boundary conditions, these simulations are performed in much the same way as those in §4.2. However, it is necessary to replace the two-dimensional Simpson integration over the particle surfaces with a more efficient Gauss quadrature approach. The Gauss points on the sphere surfaces are arranged in six circular rings, with 12 Gauss points per ring, as described by Abramowitz & Stegun (1965). This quadrature scheme is approximately 20 times faster than the Simpson rule, and is sufficient to allow accurate reproduction of all the results presented in §4.2.

Schematic diagrams of the locations of the spheres at various times are given in figure 8(*a–e*) for several simulations with $N = 25$. The sample initial condition shown in figure 8(*a*) is obtained by using a random number generator to identify 25 non-overlapping but otherwise random positions. A different initial condition is used for each simulation, the example depicted in figure 8(*a*) corresponding to $\phi = 0.15$ and $N = 25$. The other illustrations are all calculated at later times (i.e. $t = 106$ in figure 8*b*, $t = 365$ in figure 8*c*, $t = 485$ in figure 8*d*) and $t = 500$ in figure 8*e*, when the particles have clustered together to a significant extent. In general, the clustering process occurs faster at higher volume fractions and at higher Deborah numbers, because the elastic contribution to the particle interactions is strongest under those conditions. Some clustering is observed in every simulation performed. However, the size of the clusters depends on the simulation conditions, with higher volume fractions and higher Deborah numbers leading to larger clusters. The clusters are not isotropic, but are elongated in the direction of sedimentation. This formation of elongated clusters is qualitatively similar to the observations of Joseph *et al.* (1992, 1994).

It is to be emphasized that the results shown in figure 8(*a–e*) are not anomalous, but rather are typical of what is observed in all the simulations at the corresponding conditions. Newtonian simulations run at the same conditions show no signs of such clustering behaviour. As a practical matter, we note that the formation of these clusters

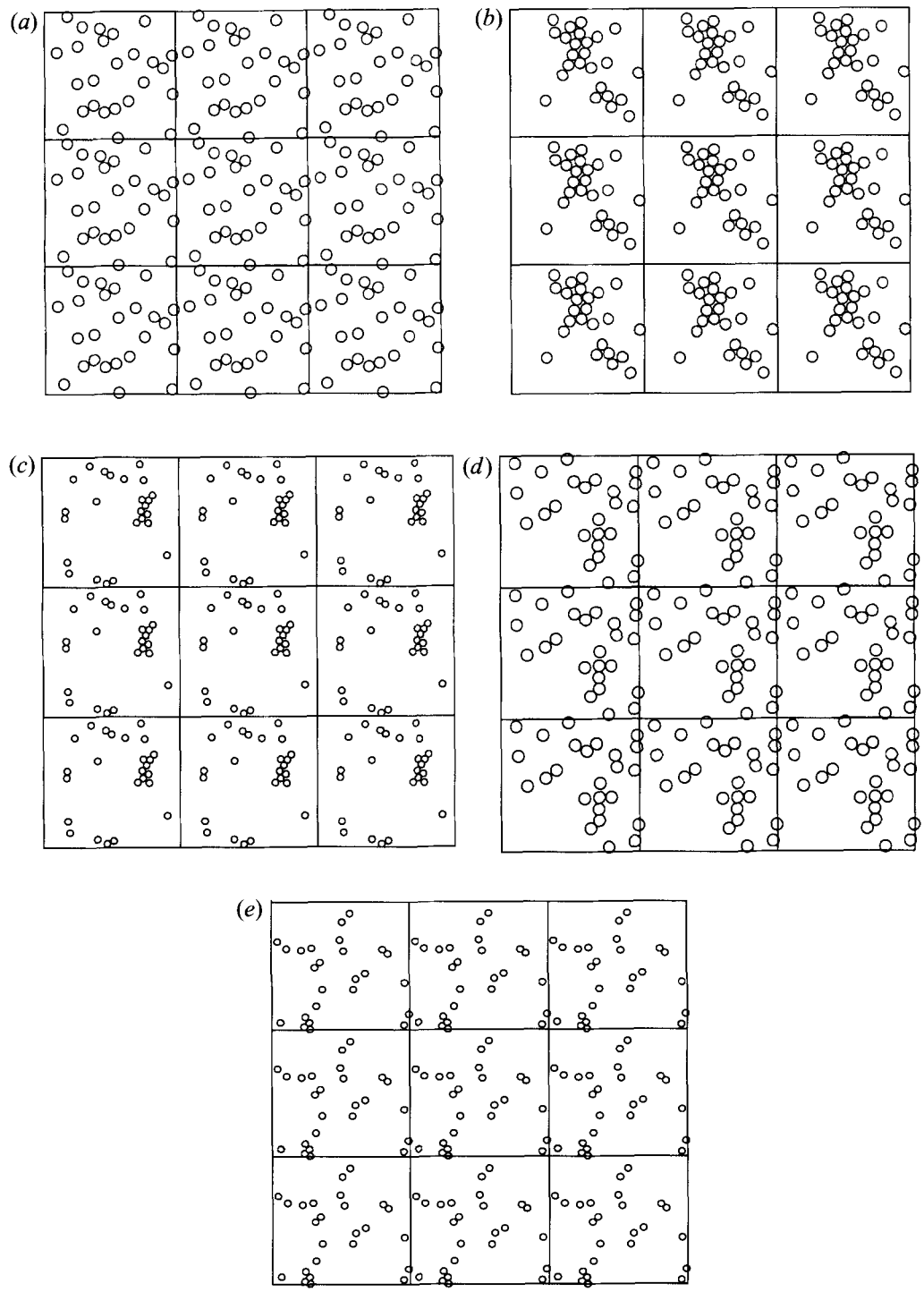

FIGURE 8. Sample configurations for simulations with 25 spheres: (*a*) initial condition for $\phi = 0.15$; (*b*) $De = 0.1$ and $\phi = 0.15$ at $t = 106$; (*c*) $De = 0.1$ and $\phi = 0.05$ at $t = 365$; (*d*) $De = 0.01$ and $\phi = 0.15$ at $t = 485$; (*e*) $De = 0.01$ and $\phi = 0.05$ at $t = 500$.

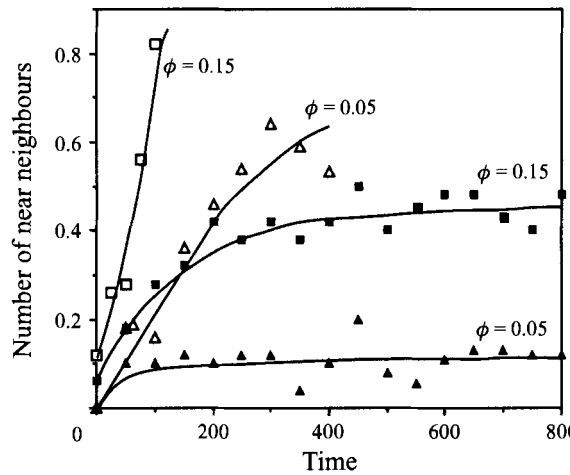

FIGURE 9. Average number of near neighbours as a function of time.

makes it necessary to use progressively smaller time increments to avoid particle overlap. The time steps used in these simulations ranged from 0.25 to 0.01. Small amounts of overlap are handled by moving the two spheres along their line-of-centres to a separation of 10^{-7}. However, in a large cluster such a process can lead to overlap with a third sphere, and hence the need for progressively smaller time steps.

In order to compare the behaviour of the suspensions under the four conditions tested, the average number of near neighbours is plotted as a function of time in figure 9, where the open symbols correspond to $De = 0.1$ and the solid symbols to $De = 0.01$. Here a 'near neighbour' is defined as a sphere within a dimensionless distance of 0.1 of another sphere. Only the 25-sphere simulations are represented in the curves shown. The rapid clustering that occurs at $De = 0.1$ and $\phi = 0.15$ is clearly evident in the upper curve, which shows that at a dimensionless time of 100 nearly every sphere is close to at least one other sphere. Similar but less rapid clustering takes place at $De = 0.1$ and $\phi = 0.05$. Interestingly, upon decreasing the Deborah number by a factor of ten a steady state is reached, where clustering is still evident but the system appears to be stable.

In figure 10 is shown the angular average of the pair distribution function $g(r, t)$ for the simulations where $N = 25$, $De = 0.1$ and $\phi = 0.15$. This distribution function is defined here as a time-dependent quantity because these simulations do not reach steady state. The usefulness of $g(r, t)$ in this context is merely to provide a concise description of the formation of clusters under one set of conditions. The absence of any structure in the initial condition and the subsequent formation of structure as evidenced by peaks at spacings of one diameter are clearly apparent. The progression toward the final, clustered state can be seen by examining the curves plotted from different times in the simulation.

The results suggest that a small amount of elasticity in a fluid can generate significant changes in the microstructure of monomodal suspensions, even at very low volume fractions. Although one expects the results shown here to be dependent on the size of the periodic unit cell, the simulations do capture the qualitative features of the aggregation process. Statistical fluctuations in the local particle concentration cause the aggregative contribution of elasticity in the fluid to be sufficiently strong to initiate cluster formation. The clusters themselves then interact, forming larger clusters under conditions where the Deborah number and area fraction are high enough. The fact that

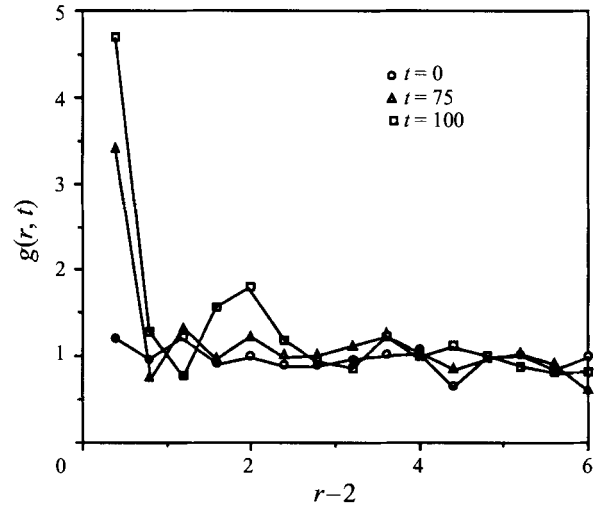

FIGURE 10. Angular-averaged, time-dependent pair distribution functions $g(r, t)$ for $t = 0$, 75 and 100 at $De = 0.1$ and $\phi = 0.15$.

the clusters at $De = 0.01$ seem to reach a steady state, as indicated by figure 9, is possibly due to the effects of hydrodynamic dispersion. A quantitatively accurate calculation of the cluster size distribution undoubtedly requires simulations with a value of N considerably greater than the 25 spheres used in this work.

This work was supported by grant CTS-94-00737 from the National Science Foundation.

REFERENCES

ABRAMOWITZ, M. & STEGUN, I. A. 1965 *Handbook of Mathematical Functions*. Dover.

ALLEN, E. & UHLHERR, P. H. T. 1989 Nonhomogeneous sedimentation in viscoelastic fluids. *J. Rheol.* **33**, 627.

BARTRAM, E., GOLDSMITH, H. L. & MASON, S. G. 1975 Particle motions in non-Newtonian media. III. Further observations in elasticoviscous fluids. *Rheol. Acta* **14**, 776.

BIRD, R. B. B., ARMSTRONG, R. C. & HASSAGER, O. 1987 *Dynamics of Polymeric Liquids*. J. Wiley and Sons.

BISGAARD, C. 1983 Velocity fields around spheres and bubbles investigated by laser-doppler anemometry. *J. Non-Newtonian Fluid Mech.* **12**, 283.

BRADY, J. F. & BOSSIS, G. 1988 Stokesian Dynamics. *Ann. Rev. Fluid Mech.* **20**, 111.

BRADY, J. F., PHILLIPS, R. J., LESTER, J. C. & BOSSIS, G. 1988 Dynamic simulation of hydrodynamically interacting suspensions. *J. Fluid Mech.* **195**, 257.

BRUNN, P. 1976 The slow motion of a sphere in a second-order fluid. *Rheol. Acta* **15**, 163.

BRUNN, P. 1977*a* The slow motion of a rigid particle in a second-order fluid. *J. Fluid Mech.* **82**, 529.

BRUNN, P. 1977*b* Interaction of spheres in a viscoelastic fluid. *Rheol. Acta* **16**, 461.

BRUNN, P. 1980 The motion of rigid particles in viscoelastic fluids. *J. Non-Newtonian Fluid Mech.* **7**, 271.

BUSH, M. B. & PHAN-THIEN, N. 1984 Drag force on a sphere in creeping motion through a Carreau model fluid. *J. Non-Newtonian Fluid Mech.* **16**, 303.

CHAN, P. C.-H. & LEAL, L. G. 1977 A note on the motion of a spherical particle in a general quadratic flow of a second-order fluid. *J. Fluid Mech.* **82**, 549.

CHANG, C, Y. & POWELL, R. L. 1994 Self-diffusion of bimodal suspensions of hydrodynamically interacting spherical particles in shearing flow. *J. Fluid Mech.* **281**, 51.

CHHABRA, R. P. & UHLHERR, P. H. T. 1980 Creeping motion of spheres through shear thinning elastic fluids described by the Carreau viscosity equation. *Rheol. Acta* **19**, 187.

CHIBA, K., SONG, K.-W. & HORIKAWA, A. 1986 Motion of a slender body in quiescent polymer solutions. *Rheol. Acta* **25**, 380.

DURLOFSKY, L., BRADY, J. F. & BOSSIS, G. 1987 Dynamic simulation of hydrodynamically interacting particles. *J. Fluid Mech.* **180**, 21.

GANATOS, P., PFEFFER, R. & WEINBAUM, S. 1978 A numerical-solution technique for three-dimensional Stokes flows, with application to the motion of strongly interacting spheres in a plane. *J. Fluid Mech.* **84**, 79.

GAUTHIER, G., GOLDSMITH, H. L. & MASON, S. G. 1971 Particle motions in non-Newtonian media. I. Couette flow. *Rheol. Acta* **10**, 344.

HAPPEL, J. & BRENNER, H. 1986 *Low Reynolds Number Hydrodynamics*. Martinus-Nijhoff.

HIGHGATE, D. J. & WHORLOW, R. W. 1969 End effects and particle migration effects in concentric cylinder rheometry. *Rheol. Acta* **8**, 142.

HOCKING, L. M. 1964 The behaviour of clusters of spheres falling in a viscous fluid. Part 2. Slow motion theory. *J. Fluid Mech.* **20**, 129.

JOSEPH, D. D., LIU, Y. J., POLETTO, M. & FENG, J. 1994 Aggregation and dispersion of spheres falling in viscoelastic liquids. *J. Non-Newtonian Fluid Mech.* **54**, 45.

JOSEPH, D. D., NELSON, J., HU, H. H. & LIU, Y. J. 1992 Competition between inertial pressures and normal stresses in the flow induced anisotropy of solid particles. In *Theoretical and Applied Rheology* (ed. P. Moldenaers & R. Keunings). Elsevier.

KARNIS, A. & MASON, S. G. 1967 Particle motions in sheared suspensions. XIX. Viscoelastic media. *Trans. Soc. Rheol.* **10**, 571.

KIM, S. 1986 The motion of ellipsoids in a second order fluid. *J. Non-Newtonian Fluid Mech.* **21**, 255.

KIM, S. & KARRILA, S. J. 1991 *Microhydrodynamics*. Butterworth-Heinemann.

LEAL, L. G. 1975 The slow motion of slender rod-like particles in a second-order fluid. *J. Fluid Mech.* **69**, 305.

LEAL, L. G. 1979 The motion of small particles in non-Newtonian fluids. *J. Non-Newtonian Fluid Mech.* **5**, 33.

LIU, Y. J. & JOSEPH, D. D. 1993 Sedimentation of particles in polymer solutions. *J. Fluid Mech.* **255**, 565.

LOVALENTI, P. M. & BRADY, J. F. 1993 The hydrodynamic force on a rigid particle undergoing arbitrary time-dependent motion at small Reynolds number. *J. Fluid Mech.* **256**, 561.

LUNSMANN, W. J., GENIESER, L., ARMSTRONG, R. C. & BROWN, R. A. 1993 Finite element analysis of steady viscoelastic flow around a sphere in a tube – calculations with constant viscosity models. *J. Non-Newtonian Fluid Mech.* **48**, 63.

MCKINLEY, G. H., ARMSTRONG, R. C. & BROWN, R. A. 1993 The wake instability in viscoelastic flow past confined cylinders. *Phil. Trans. R. Soc. Lond.* A **344**, 265.

MICHELE, J., PATZOLD, R. & DONIS, R. 1977 Alignment and aggregation effects in suspensions of spheres in non-Newtonian media. *Rheol. Acta* **16**, 317.

PETIT, L. & NOETINGER, B. 1988 Shear-induced structures in macroscopic dispersions. *Rheol. Acta* **27**, 437.

PHILLIPS, R. J., BRADY, J. F. & BOSSIS, G. 1988*a* Hydrodynamic transport properties of hard-sphere dispersions. I. Suspensions of freely mobile particles. *Phys. Fluids* **31**, 3462.

PHILLIPS, R. J., BRADY, J. F. & BOSSIS, G. 1988*b* Hydrodynamic transport properties of hard-sphere dispersions. II. Porous media. *Phys. Fluids* **31**, 3473.

RIDDLE, M. J., NARVAEZ, C. & BIRD, R. B. 1977 Interactions between two spheres falling along their line of centers in a viscoelastic fluid. *J. Non-Newtonian Fluid Mech.* **2**, 23.

RUSSEL, W. B., SAVILLE, D. A. & SCHOWALTER, W. R. 1989 *Colloidal Dispersions*. Cambridge University Press.

SATRAPE, J. V. & CROCHET, M. J. 1994 Numerical simulation of the motion of a sphere in a Boger fluid. *J. Non-Newtonian Fluid Mech.* **55**, 91.

WEINBAUM, S., GANATOS, P. & ZONG-YI, Y. 1990 Numerical multipole and boundary integral equation techniques in Stokes flow. *Ann. Rev. Fluid Mech.* **22**, 275.